Energy Efficiency of Permeate Gap and Novel Conductive Gap Membrane Distillation[1]

Jaichander Swaminathan[a], Hyung Won Chung[a], David M. Warsinger[a], Faisal Al-Marzooqi[b], Hassan A. Arafat[b], John H. Lienhard V [2a]

[a] *Rohsenow Kendall Heat Transfer Laboratory, Department of Mechanical Engineering, Massachusetts Institute of Technology, Cambridge MA 02139-4307 USA*
[b] *Institute Center for Water and Environment (iWater), Department of Chemical and Environmental Engineering, Masdar Institute of Science and Technology, PO Box 54224, Abu Dhabi, United Arab Emirates*

Abstract

This work presents numerical modeling results and flux experiments for a novel membrane distillation configuration called conductive gap membrane distillation (CGMD), as well as permeate gap membrane distillation (PGMD). CGMD has a conductive spacer in the gap between the membrane and condensing surface rather than more commonly used insulating materials. Flux measurements with two experimental systems are used to validate the numerical models for PGMD and CGMD. PGMD has 20% higher GOR (energy efficiency) than an air gap membrane distillation (AGMD) system of the same size, whereas CGMD can have two times higher GOR than even PGMD. Increasing gap effective thermal conductivity in CGMD has negligible benefits beyond $k_{\text{gap}} \approx 10$ W/m·K under the conditions of this study. The direction of pure water flow in the gap has a significant influence on overall system energy efficiency, especially in the case of CGMD. Using a countercurrent configuration for the pure water flow in the gap relative to the cold stream leads to 40% higher GOR than flow cocurrent with the cold water stream.

Keywords: Membrane Distillation, Energy Efficiency, Permeate Gap, Conductive Gap

[1] Citation: J. Swaminathan, H.W. Chung, D.M. Warsinger, F.A. AlMarzooqi, H.A. Arafat, J.H. Lienhard, "Energy efficiency of permeate gap and novel conductive gap membrane distillation," *J. Membr. Sci.*, Vol. 502, pp. 171–178, 15 March 2016, http://dx.doi.org/10.1016/j.memsci.2015.12.017
[2] Corresponding author: lienhard@mit.edu

Nomenclature

Roman Symbols

A	Membrane area, m^2
B	Membrane permeability, kg/m^2 s Pa
c	Salt concentration, g/kg
d	Depth of channel, m
dA	Elemental area, m^2
GOR	Gained Output Ratio
h	Specific enthalpy, kJ/kg
h_{fg}	Enthalpy of vaporization, J/kg
J	Permeate flux, kg/m^2 s
k_{mass}	Mass transfer coefficient, m/s
L	Length of module, m
MW	Molar mass, kg/mol
$\dot{m}$	Mass flow rate, kg/s
$\dot{Q}$	Heat transfer rate, W
$\dot{q}$	Heat flux, W/m^2
P	Pressure, Pa
p^{vap}	Vapor Pressure, Pa
T	Temperature, °C
T_0	Ambient temperature, °C
w	Width, m

Greek Symbols

δ_{m}	Membrane thickness, m
ϕ	Membrane Porosity
ρ	Density

Subscripts

b	Stream bulk
br	Brine stream
c	Cold stream
f	Feed (hot) stream
g	Gap
h	Heater
in	Inlet

m	Membrane surface
out	Outlet
p	Product stream
sat	Saturation
w, wall	Condensing surface

1. Introduction

1.1. Membrane Distillation

Membrane distillation (MD) is a thermal desalination technology that has received increased attention for small scale, renewable-energy-driven desalination applications as well as for treating high salinity brines. Scalability, the ability to handle high salinity feed streams, and relatively high fouling resistance are some of the advantages of the MD process. Several MD configurations with relative advantages and disadvantages have been proposed in the literature. The four common MD configurations include air gap (AGMD), direct contact (DCMD), vacuum (VMD) and sweeping gas membrane distillation (SGMD) [1, 2]. In addition, other configurations have been suggested recently, including the permeate (liquid or water) gap MD (PGMD), and material gap membrane distillation (MGMD) [3]. Several multi-staged configurations based on the above designs have also been proposed in literature and commercially implemented [4].

The fundamental principle of operation of all these configurations is the same. Separation is achieved through evaporation of the more volatile component of a mixture. When used for desalination, pure vapor preferentially passes through the pores of a hydrophobic membrane that prevents liquid feed from passing through. The different configurations of MD vary based on how this vapor is captured and condensed to obtain pure water. In the case of DCMD, cooler pure water flows on the other side of the membrane, countercurrent to the feed, and the vapor condenses into this stream and warms it up. The warm pure water stream would then be passed through a heat exchanger to preheat incoming salt water [5, 6]. DCMD is the oldest MD configuration proposed [7]. In AGMD, the vapor condenses on a condensing plate that is cooled by the incoming feed. The feed thereby gets preheated within the module by the condensing vapor, hence recovering some of the energy input. The air gap between the membrane and the condensing surface is meant to reduce the sensible heat loss from the hot to the cold side [8].

In the case of SGMD and VMD, the condensation happens outside the MD module. The sweeping air gets heated and humidified before leaving the module in SGMD, and in VMD, the vacuum pump would draw out relatively pure vapor in the case of VMD. This is passed through a condenser or vapor trap to recover pure liquid water [9]. Recently, a system using an aspirator was proposed to more efficiently recover the product water in VMD systems [10], eliminating the vacuum pump and concerns associated with incomplete condensation.

1.2. Energy Efficiency

Energy is supplied to MD systems both in the form of heat and work. Work transfer is usually used to achieve fluid flow through the channels. Heat is required to increase the temperature of the feed liquid and thereby enabling evaporation of water. Heat energy consumption by far exceeds pumping power requirements under normal operating conditions. Energy consumption in MD has been relatively higher than that of other desalination technologies as illustrated by Mistry et al. [11]. As a result, MD companies have focused on applications with available waste heat energy, from power plants or other sources [4, 12]. MD is also readily

coupled with renewable and waste heat sources due to its ability to operate at low temperatures and still achieve desalination.

Energy efficiency is analyzed as gained output ratio (GOR) (Eq. 1):

$$\mathrm{GOR} = \frac{\dot{m}_\mathrm{p} h_\mathrm{fg}}{\dot{Q}_\mathrm{h}} \tag{1}$$

Most MD systems in practice have been restricted to GORs of less than about 4-6 [4, 13]. In contrast, large scale thermal desalination systems such as multi-stage flash and multi-effect distillation, which may have significantly more complicated designs often have GOR higher than about 7-10 [14]. Increasing the GOR of MD close to these values would make MD more competitive with these conventional technologies.

The GOR of single stage MD configurations has been previously analyzed and compared by Summers et al. [5]. While single stage VMD systems are restricted to GOR below 1, single stage SGMD also does not achieve GOR beyond about 4 [9]. In contrast, DCMD and AGMD are relatively simple systems, and were shown to be capable of achieving higher GORs [5, 15, 16, 17].

1.3. Permeate Gap Membrane Distillation

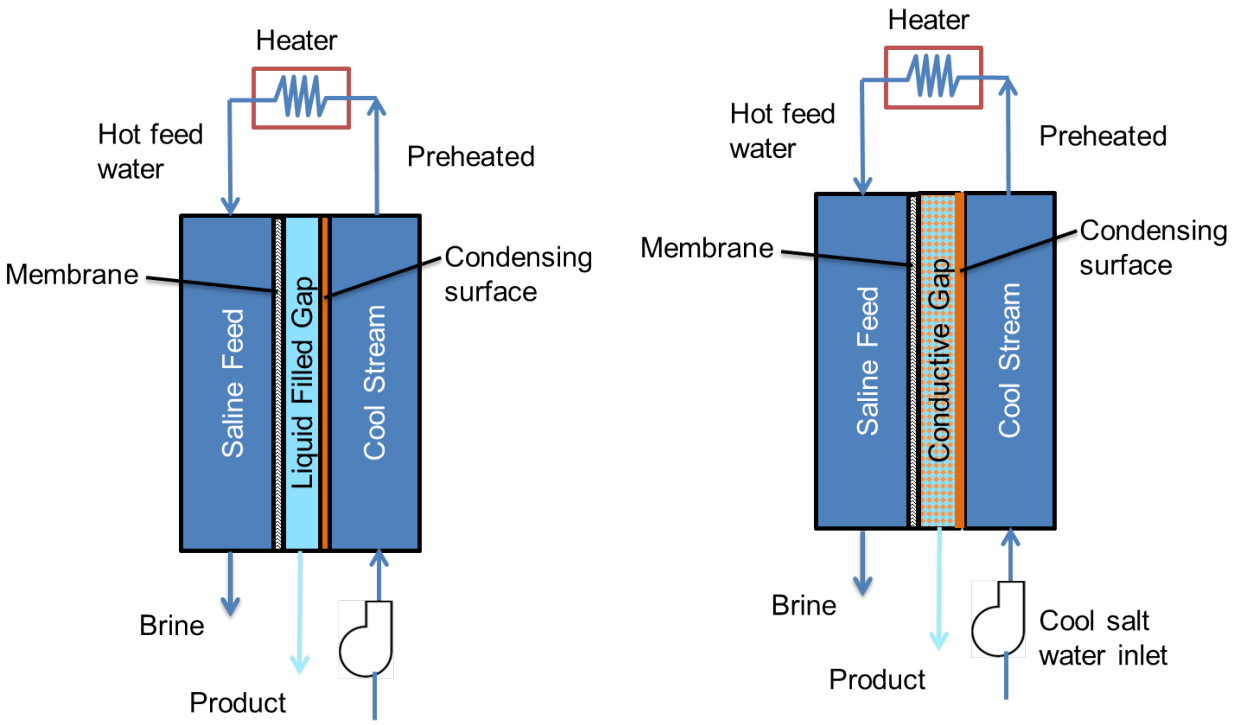

(a) Permeate Gap Membrane Distillation

(b) Conductive Gap Membrane Distillation proposed as a modification of PGMD

Figure 1: MD configurations analyzed in this study

Permeate Gap MD is also referred to as Water Gap and Liquid Gap MD. Simply, it can be understood as a modification of AGMD where the gap between the membrane and the condensing surface is filled

with permeate water (Fig. 1a). PGMD has shown improved fluxes compared to AGMD [8, 18, 19] as have other modifications such as material gap MD systems with sand added to the gap [3]. A clear comparison of GOR between AGMD and PGMD has not been established, though commercial spiral wound PGMD modules have achieved higher GOR . Winter et al. [20] suggested PGMD as a modification of DCMD with internal heat recovery by separation of the distillate from the coolant. Therefore the coolant can be any other liquid, such as incoming feed water. They note that "The presence of the distillate channel reduces sensible heat losses due to an additional heat transfer resistance. An additional effect is the reduction of the effective temperature difference across the membrane, which slightly lowers the permeation rate." PGMD can therefore be intuitively placed between AGMD and DCMD with intermediate thermal resistance of the gap, thereby having lower sensible heat transfer to the permeate as compared to DCMD, but perhaps more heat loss than AGMD. A hollow fiber MD system in PGMD configuration was experimentally analyzed by Singh et al. [21], where the condensate from one AGMD module was passed into another module. Singh et al. note that the second module would perform between AGMD and DCMD when the gaps are filled with condensate. Hollow fiber systems with high packing density may also lead to much lower effective gap sizes [22] and sections of the module may have pure water extending across the narrow gaps between membrane and non-porous fibers. While the focus of the present work is on modeling flat sheet and similar spiral-wound MD systems, the overall trends are applicable to hollow fiber MD systems as well.

1.4. Conductive Gap Membrane Distillation

Conductive gap MD (CGMD) is suggested as a novel MD configuration (Fig. 1b). In CGMD, the overall thermal conductance of the gap is increased. One way of achieving this is to insert a high conductivity material (such as a metal mesh) into the gap of a PGMD system. Increasing the conductivity of the gap in hollow fiber MD systems by inserting high conductivity materials was suggested by Ma et al. [23] in 2010. This is in contrast to other systems proposed in the literature such as material gap MD where low conductivity materials such as sand were added to the gap region [3]. This also contradicts the conventional wisdom and the historical development in the field towards developing MD configurations with lower sensible heat loss than DCMD [24], such as the the evolution from DCMD to AGMD or PGMD. Possible implementations involve using a metal spacer instead of a plastic spacer, or implementing fins on the conductive surface extending up to the membrane to increase the net conductivity of the gap. The gap is filled with pure water, similar to the PGMD system. Vapor would condense immediately as it leaves the membrane. The energy is conducted through the gap into the cold stream, preheating it. While this configuration may have a higher sensible heat loss than even PGMD, perhaps close to that of a DCMD system, for a given membrane area and feed flow rate, it rejects brine at a lower temperature and correspondingly achieves higher preheating of the cold stream. This could therefore result in a higher overall GOR.

In this study, we use numerical modeling to investigate the energy efficiency of PGMD and CGMD systems. The results are compared to previously published results for other conventional MD configurations

under the same operating conditions. The effect of pure water flow direction in the gap is evaluated. The effect of gap conductivity and membrane material conductivity on GOR is studied.

2. Numerical Modeling

2.1. Review

Several MD models with varying degrees of complexity have been developed to understand the effect of system parameters on flux [25, 26]. Fewer, however, have analyzed energy efficiency [6, 27, 28]. The modeling approach followed in this paper is very similar to that found in Summers et al. [5]. As a result, only the new features of the modeling are discussed in detail.

A one-dimensional model of the MD modules is studied, where properties vary along the length of the module, but are constant along the width (direction into the page). In the depth direction, property variations due to transport processes are evaluated by considering the temperature and concentration boundary layers. The bulk properties of the fluids are assumed equal to the value at the fluid interior; the boundary layers are assumed to be thin, but not negligible. Mass, and energy conservation equations are solved for each computational cell coupled with property evaluations performed using built-in functions on Engineering Equation Solver (EES) [29].

The overall computational cell is shown in Fig. 2.

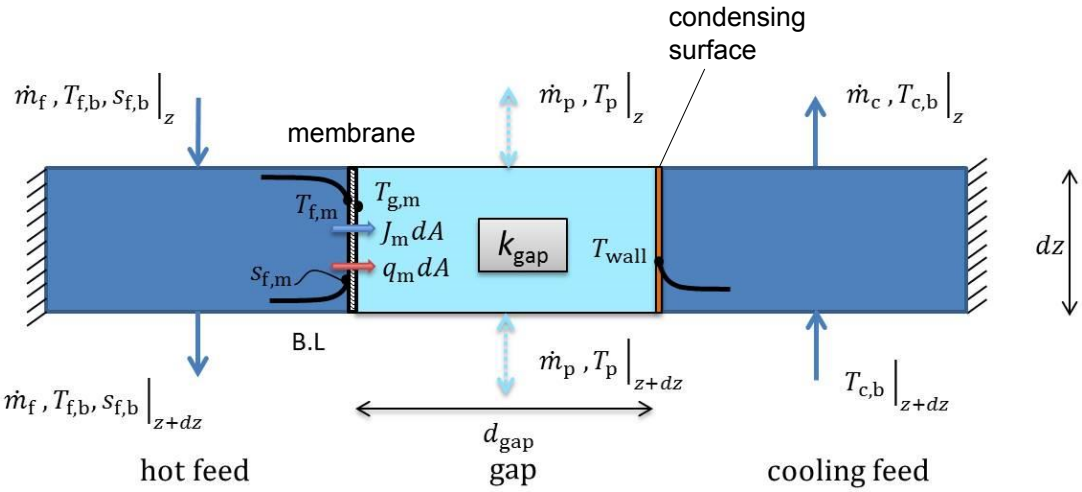

Figure 2: PGMD computational cell

2.2. Feed Channel

Modeling of the feed channel is common to both configurations. A concentration boundary layer is incorporated into the feed channel model to account for desalination of salt water and capture second order effects associated with salinity of the feed. The film model of concentration polarization (Eq. 2) is used to relate the salt concentrations at the membrane interface ($c_{\mathrm{f,m}}$) to the bulk concentration ($c_{\mathrm{f,b}}$), effective mass transfer coefficient (k) in the channel and vapor flux thorough the membrane (J):

$$\frac{c_{\mathrm{f,m}}}{c_{\mathrm{f,b}}} = \exp\left(\frac{J}{\rho_{\mathrm{f}} k_{\mathrm{mass}}}\right) \tag{2}$$

The effect of dissolved salt on the vapor pressure of water is captured using Raoult's law (Eq. 3):

$$p_{\mathrm{f,m}}^{\mathrm{vap}} = P_{\mathrm{sat}}\left(T_{\mathrm{f,m}}\right) \times \left(1 - \frac{\frac{2c_{\mathrm{f,m}}}{MW_{\mathrm{solute}}}}{\frac{2c_{\mathrm{f,m}}}{MW_{\mathrm{solute}}} + \frac{1000 - c_{\mathrm{f,m}}}{MW_{\mathrm{water}}}}\right) \tag{3}$$

The difference in vapor pressure across the membrane is the driving force for water vapor transfer as shown in Fig. 2. The effect of salt content on the enthalpy of the feed solution is not modeled in detail since we are focusing on low salinity conditions where these secondary effects are negligible. The effect of salt on other thermophysical properties of the streams is not modeled. At close to seawater salinities considered in this study, the reduction in vapor pressure is the only thermally significant effect.

The flux through the membrane is calculated locally from the vapor pressure difference and the membrane permeability coefficient, B:

$$J = B \times \left(p_{\mathrm{f,m}}^{\mathrm{vap}} - p_{\mathrm{g,m}}^{\mathrm{vap}}\right) \tag{4}$$

2.3. Gap

The region between the membrane and the condensing surface will be referred to as the gap. For air gap Summers et al. [5] presented a vapor diffusion with air counter diffusion model. For PGMD and CGMD, similar to the case of DCMD, vapor condenses immediately upon exiting the membrane pores into a stream of pure water. From here, the heat is convected across the gap into the condensing surface. In this study, the water flow rate is assumed to be relatively low and hence energy transfer across the gap is approximated by conduction across the gap (5):

$$\dot{q}_{\mathrm{gap}} = \frac{k_{\mathrm{gap}}}{d_{\mathrm{gap}}} \times \left(T_{\mathrm{g,m}} - T_{\mathrm{w}}\right) \tag{5}$$

Depending on the direction of water flow in the gap, $\dot{q}_{\mathrm{gap}}$ would be different.In the case of crossflow configuration, the water produced at any given location along the length would flow perpendicularly out of the module (in this case, into or out of the plane of the paper, as shown in Fig. 4). On the other hand, the flow can also be countercurrent to the cold stream or parallel to the flow stream. The corresponding equations for cell number n are given below (cell number 1 at the hot side):

$$
\begin{aligned}
\dot{q}^n_{\text{gap,cross}} &= J^n h_v\left(T^n_{\text{f,m}}\right) + q^n_{\text{m}} - J^n h_l\left(T^n_{\text{p}}\right) \\
\dot{q}^n_{\text{gap,countercurrent}} &= J^n h_v\left(T^n_{\text{f,m}}\right) + q^n_{\text{m}} + \left[\dot{m}^{n-1}_{\text{p}} h_l\left(T^{n-1}_{\text{p}}\right) - \dot{m}^n_{\text{p}} h_l\left(T^n_{\text{p}}\right)\right]/dA \\
\dot{q}^n_{\text{gap,parallel}} &= J^n h_v\left(T^n_{\text{f,m}}\right) + q^n_{\text{m}} + \left[\dot{m}^{n+1}_{\text{p}} h_l\left(T^{n+1}_{\text{p}}\right) - \dot{m}^n_{\text{p}} h_l\left(T^n_{\text{p}}\right)\right]/dA
\end{aligned}
\tag{6}
$$

In the case of PGMD, the gap is filled with water with some plastic spacers often used to support the membrane. On the other hand, in the case of conductive gap MD, conductive materials are used to enhance the conductivity of the region. The effective thermal conductivity of this gap (k_{gap}) would therefore be a function of the conductivities of water and additional material in the gap as well porosity and geometry of the region. In this study, $k_{\text{gap}} = 0.6$ W/m-K is used for PGMD and $k_{\text{gap}} = 10$ W/m-K is used for reporting CGMD results.

The baseline conditions for the numerical model are shown in Table 1.

Table 1: Baseline values of parameters

No.	Variable	Value	Units
1	$T_{\text{f,in}}$	85	°C
2	$T_{\text{c,in}}$	27	°C
3	$\dot{m}_{\text{f,in}}$	1	kg/s
4	$c_{\text{f,in}}$	35	ppt
5	L	60	m
6	w	0.7	m
7	$d_{\text{f}}, d_{\text{c}}$	0.004	m
8	d_{gap}	0.001	m
9	k_{gap}(PGMD)	0.6	W/m-K
10	k_{gap}(CGMD)	10	W/m-K
11	B	16×10^{-7} [5]	kg/m^2 s Pa

3. Validation

The numerical modeling framework presented above has been validated for AGMD and DCMD in the past [5]. PGMD experiments were carried out using the AGMD apparatus described in detail elsewhere [18, 30]. The apparatus was used to study PGMD by collecting water from the top, hydrostatically forcing the gap region to be flooded with pure water. Experiments were conducted at different values of $T_{\text{f,in}}(40, 50, 60, 70\,^{\circ}\text{C})$

and $T_{c,in}(17, 20, 25\,^{\circ}\mathrm{C})$. For the numerical model predictions, an effective gap conductivity of $k_{gap} = 0.6$ W/m-K and effective gap thickness of 1 mm were used. Under similar conditions compared to PGMD, the flux for AGMD is about 20% lower at higher $T_{f,in}$ and more than 50% lower at lower temperatures. This result is comparable to results in the literature that show that flux for liquid gap MD is higher than that of AGMD. The magnitude of improvement in this study may be smaller since a smaller gap thickness is used, resulting in lower resistance in the case of AGMD.

The results comparing the numerical modeling predictions against the experimental results are shown in Fig. 3a. Each set of three data points corresponds to one value of hot side temperature.

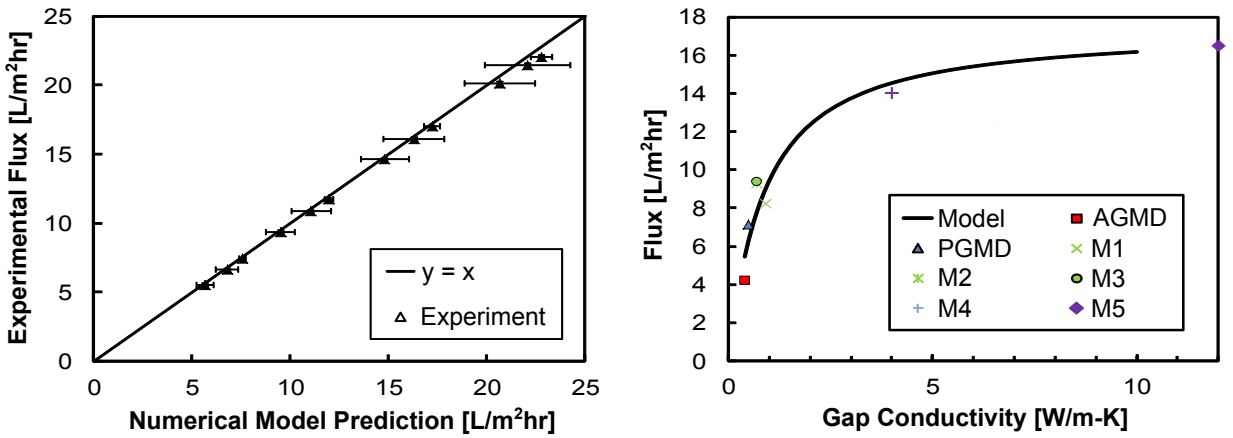

(a) Experimental flux compared with numerical modeling results. $T_{f,in} = 40, 50, 60, 70\,^{\circ}\mathrm{C}$, $T_{c,in} = 17, 20, 25\,^{\circ}\mathrm{C}$

(b) Experimental flux measurements at different values of gap conductivity

Figure 3: Model validation with experimental flux measurements

Further validation of the model for the effect of gap conductivity in CGMD configuration was carried out using a modified Sterlitech apparatus described in [31] and the results are shown in Fig. 3b. In the figure, M1 to M5 correspond to different types of metal meshes used in the gap which is about 2-4 mm thick. M1 to M3 are woven aluminum mesh spacers (McMaster-Carr part numbers 9227T53, 9227T56, 9227T57). M4 is a porous Duocel Aluminum material (ERGAerospace part number 6101-T6) hammered down to half its thickness and covered by a thin brass mesh to protect the membrane. M5 is a specially manufactured copper plate with fins. The gap conductivity in the case of M5 is likely to be much higher, but since the increase in flux is negligible at higher conductivities, the point is plotted at the edge of the plot.

These results are also in overall agreement with flux results presented by Francis et al. [3] on material gap MD configurations. With the introduction of sand that has lower thermal conductivity than water, the flux was found to be lower than with only water in the gap. The opposite effect is observed in terms of flux for CGMD.

In order to validate the model for a larger system with energy recovery, data from spiral wound module analysis reported in [20] is used. The current model was run at the following conditions to compare with

reported results: ($B = 16 \times 10^{-7}\,\mathrm{kg/m^2 \cdot s \cdot Pa}$, $k_\mathrm{m} = 0.25\,\mathrm{W/m \cdot K}$, $\delta_\mathrm{m} = 70\,\mu\mathrm{m}$, $L = 7\,\mathrm{m}$, $w = 0.7\,\mathrm{m}$, $d_\mathrm{ch} = 3.2\,\mathrm{mm}$, feed flow inlet rate = 0.04166 kg/s, permeate flow in counterflow direction, $k_\mathrm{gap} = 0.5\,\mathrm{W/m \cdot K}$ (for water and a plastic spacer), $d_\mathrm{gap} = 1\,\mathrm{mm}$, $T_\mathrm{f,in} = 80\,^\circ\mathrm{C}$, $T_\mathrm{c,in} = 25\,^\circ\mathrm{C}$). The predicted specific thermal energy consumption is 158 $\mathrm{kWh/m^3}$, and the flux is 1.76 LMH. The values reported in [20] for the same operating conditions are specific thermal energy consumption of 150–160 $\mathrm{kWh/m^3}$ and a flux of about 1.5–1.6 LMH. The membrane permeability value, as well as the gap conditions were not available and were assumed. Also, the model does not account for heat loss to the environment.

4. Results and Discussion

4.1. GOR comparison, Effect of gap flow

The configuration of pure water flow in the gap can affect the performance of a PGMD or CGMD system. Figure 4 shows the different options for pure water flow in the gap. On the left, pure water in the gap flows countercurrent to the coolant fluid across the condensing plate. The opposite gap configuration is to have the pure water flow parallel to the coolant stream, as seen on the right. An intermediate design (middle) may be that of perpendicular or crossflow, where water flows in a direction perpendicular to that of cold water flow and leaves the module at several positions along the length of the module.

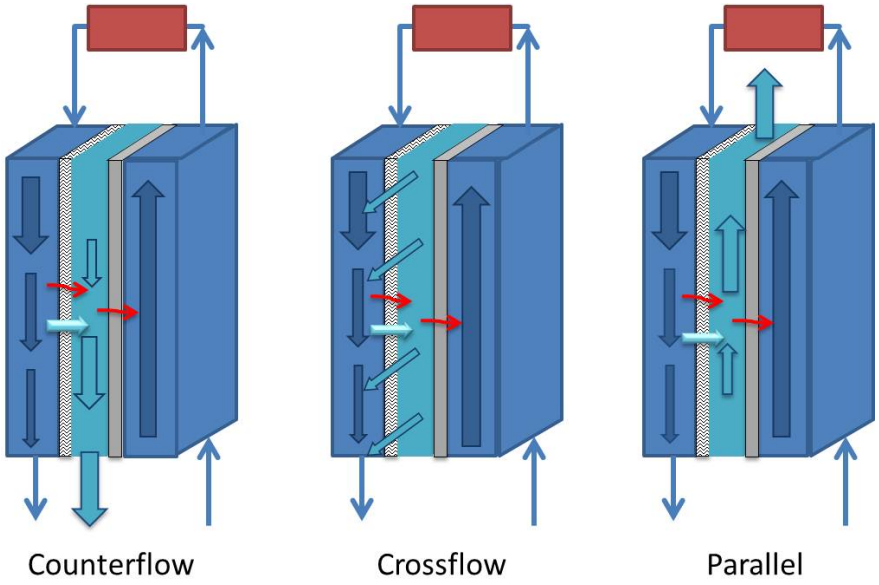

Figure 4: Illustration of various flow configurations in the gap region

The system with gap flow countercurrent to the cold stream (left) is likely to have the highest energy efficiency since the pure water would leave the system close to the cold stream inlet temperature; this is similar to the well-known behavior of a counterflow heat exchanger. On the other hand, the parallel configuration (right) would be rejecting a warm pure water stream close to the top temperature. Even

though the amount of water released is less than 8% of the feed stream, it can still have a detrimental effect on energy efficiency. The perpendicular configuration is likely to lie in between, since water is released both at warmer temperatures and cooler temperatures, and hence on average the stream is going to be of intermediate temperature.

The effect of length on GOR is shown for all three flow orientations in Fig. 5. The GOR trend is as expected. At $L = 60$ m, the GOR differs by about 1 between parallel and perpendicular and between perpendicular and countercurrent for CGMD systems (Fig. 5a). The trend is similar for PGMD systems, but the difference in magnitude of GOR differences is much smaller at about 0.2. The flux at $L = 60$ m, is 5.8 L/m^2-hr for PGMD and 6.6 L/m^2-hr for CGMD in countercurrent configuration. The higher GOR observed at larger membrane areas is accompanied by a lower flux, which is similar to the trade-off observed for DCMD systems by Gilron et al. [15]. As a result, operating at very high GOR may not be optimal.

Comparing the graphs with data from [5] for AGMD, DCMD and VMD systems over the same operating conditions, GOR of PGMD is about 20% higher than that of AGMD across the range of lengths. The GOR of CGMD in turn is about two times higher than that of PGMD.

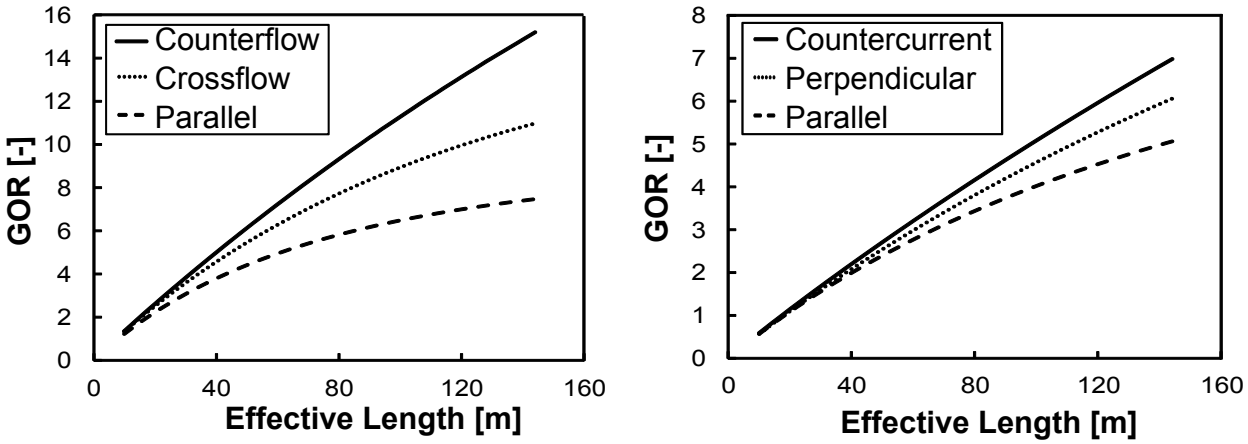

(a) Effect of gap flow direction on CGMD

(b) Effect of gap flow direction on PGMD

Figure 5: Effect of gap flow direction and system length. Other parameters set at baseline values (Table 1).

Figure 6a shows the bulk stream temperature profiles within the module for the three different flow orientations when $L = 60$ m. The temperature profiles are more straight for the counterflow case than the crossflow and parallel arrangements. The cold stream leaves at a higher temperature in the case of the counterflow configuration. This means that better preheating is achieved and hence less heat will be added from the heater, contributing to a higher GOR. Figure 6b shows the driving temperature difference between the hot and cold stream bulk temperatures along the length of the module. Interestingly, in counterflow design, the pinch point temperature difference occurs at the hot side, leading to lower external heat input, whereas in both the other configurations, the pinch point occurs at the cold end. The driving force is also relatively more constant in the counterflow design, contributing to lower entropy generation within the

module and better overall energy efficiency [32].

All subsequent results and discussions will focus on the counterflow configuration. The trends will be relatively similar for other flow configurations as well.

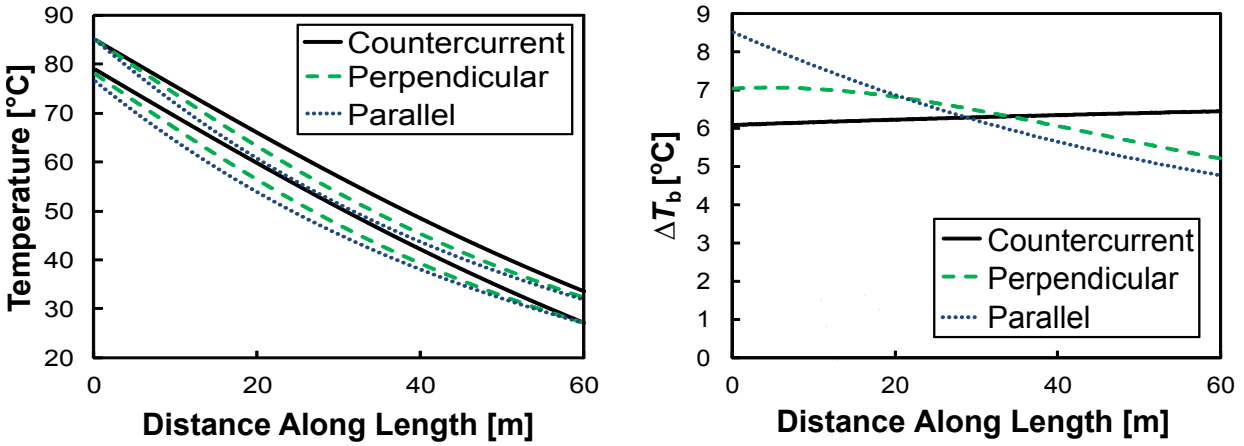

(a) Hot and cold side bulk temperature profiles for different flow configurations

(b) Temperature difference between the streams along the module

Figure 6: Effect of gap flow direction on temperature profile in CGMD. Other parameters set at baseline values (Table 1).

4.2. Effect of Gap Thermal Conductivity

Figure 7 shows the effect of gap conductivity on GOR. k_{gap} is varied over a range of 0.5 W/m-K to more than 30 W/m-K. At lower k_{gap}, an increase in the conductivity leads to significant improvements in GOR (Fig. 7) whereas beyond about $k_{\text{gap}} = 10$ W/m-K, increase in conductivity doesn't result in much further improvement.

The results shown in Fig. 7 are also applicable for analyzing PGMD with smaller gap as can be easily achieved by using a thinner spacer or packing the fibers more densely in the case of hollow fiber system. The effect of reducing the gap thickness is similar to that of increasing the conductivity of the gap. From Eq. 5, we see that the parameter of interest is the gap conductance given by $k_{\text{gap}}/\delta_{\text{gap}}$. At higher gap conductivity or lower gap thickness the system would start behaving closer to CGMD. The value of gap conductance corresponding to a $k_{\text{gap}} = 10$ W/m-K as used in this study is 10000 W/m^2-K. To achieve a similar conductance with a permeate gap system, the gap thickness would have to be 60 μm.

Figure 8 illustrates the effect of k_{gap} on $\dot{m}_{\text{p}}$ and $\dot{Q}_{\text{h}}$. $\dot{m}_{\text{p}}$ increases and $\dot{Q}_{\text{h}}$ decreases, both leading to an improvement in GOR. Among the two, the increase in $\dot{m}_{\text{p}}$ is about 15% whereas the decrease in $\dot{Q}_{\text{h}}$ is around 60%. Together, both of these effects result in the nearly 100% higher GOR for CGMD compared to PGMD, as k_{gap} increases from about 0.6 to 10 W/m-K.

The temperature profiles within the modules are illustrated in Fig. 9 and help explain the results physically. For PGMD, a relatively large difference in temperature is observed between the membrane surface and

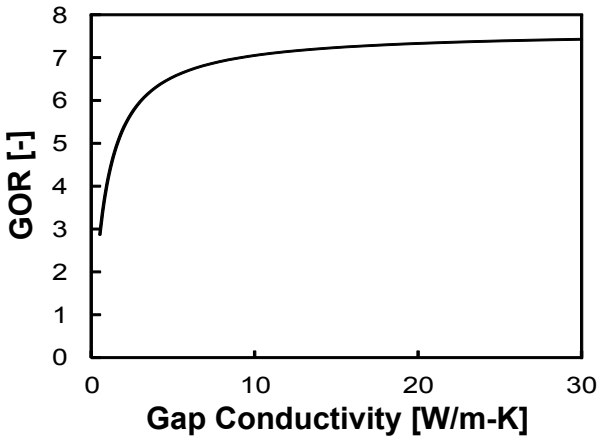

Figure 7: Energy efficiency as a function of gap conductivity = 0.5–30 W/m·K. Other parameters set at baseline values (Table 1).

the condensation plate. As a result, there is a smaller temperature difference across the membrane leading to lesser pure water production, even though the overall pinch point temperature difference between the bulk streams is much larger compared to the profile for CGMD. On the other hand, since the pinch point temperature difference is smaller in CGMD, lesser external energy supply was required too.

5. Conclusions

1. Numerical modeling shows that PGMD systems have higher GOR than AGMD. The proposed CGMD configuration with a high thermal conductivity gap has two times higher GOR than even PGMD.
2. Pure water flow in the gap countercurrent to the cold stream leads to highest energy efficiency followed in order of efficiency by crossflow and parallel configurations.
3. An increase in gap conductivity improves permeate production and GOR, with diminishing returns beyond $k \approx 10$ W/m-K in the cases considered here.
4. The main reason for improved GOR of CGMD is better energy recovery into the cold stream within the MD module.

Acknowledgments

This work was funded by the Cooperative Agreement Between the Masdar Institute of Science and Technology (Masdar Institute), Abu Dhabi, UAE and the Massachusetts Institute of Technology (MIT), Cambridge, MA, USA, Reference No. 02/MI/MI/CP/11/07633/GEN/G/00, and facilitated by the MIT Deshpande Center for Technological Innovation and the Masdar Institute Center for Innovation and Entrepreneurship (iInnovation).

The authors would like to thank MIT undergraduate students Ann M. Huston and Grace Connors for their help in preparing the manuscript and setting up the experiments.

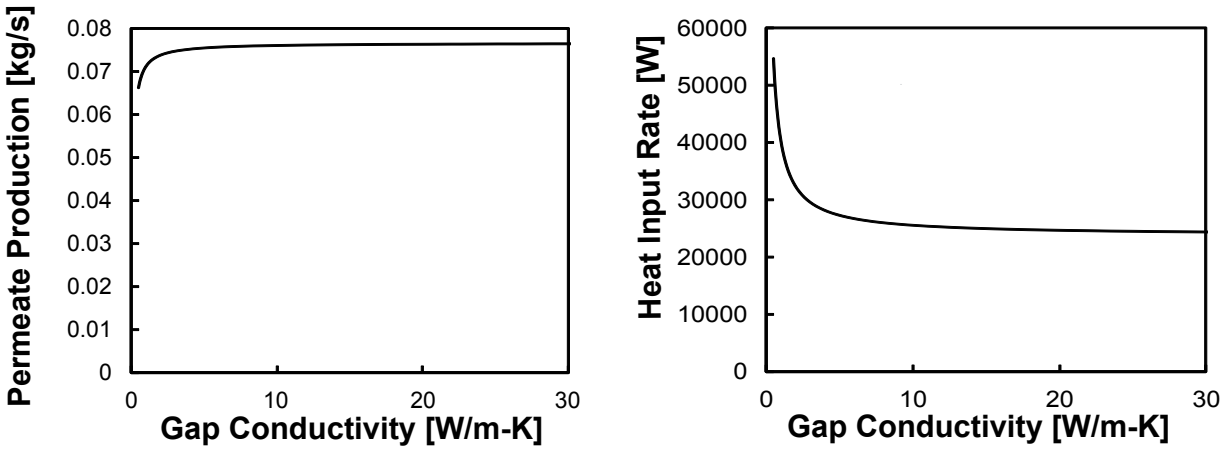

(a) Water production

(b) Heat input

Figure 8: Effect of gap conductivity on permeate production and heat input rate. Other parameters set at baseline values (Table 1).

References

[1] D. M. Warsinger, J. Swaminathan, E. Guillen-Burrieza, H. A. Arafat, J. H. Lienhard V, Scaling and fouling in membrane distillation for desalination applications: A review, Desalination 356 (2014) 294–313. doi:http://dx.doi.org/10.1016/j.desal.2014.06.031.
URL http://www.sciencedirect.com/science/article/pii/S0011916414003634

[2] A. Alkhudhiri, N. Darwish, N. Hilal, Membrane distillation: A comprehensive review, Desalination 287 (2012) 2–18. doi:10.1016/j.desal.2011.08.027.
URL http://linkinghub.elsevier.com/retrieve/pii/S0011916411007284

[3] L. Francis, N. Ghaffour, A. A. Alsaadi, G. L. Amy, Material gap membrane distillation: A new design for water vapor flux enhancement, Journal of Membrane Science 448 (2013) 240 – 247. doi:http://dx.doi.org/10.1016/j.memsci.2013.08.013.
URL http://www.sciencedirect.com/science/article/pii/S0376738813006595

[4] K. Zhao, W. Heinzl, M. Wenzel, S. Büttner, F. Bollen, G. Lange, S. Heinzl, N. Sarda, Experimental study of the Memsys vacuum-multi-effect-membrane-distillation (V-MEMD) module, Desalination 323 (2013) 150–160. doi:10.1016/j.desal.2012.12.003.
URL http://linkinghub.elsevier.com/retrieve/pii/S0011916412006509

[5] E. K. Summers, H. A. Arafat, J. H. Lienhard V, Energy efficiency comparison of single-stage membrane distillation (MD) desalination cycles in different configurations, Desalination 290 (2012) 54–66.
URL http://linkinghub.elsevier.com/retrieve/pii/S0011916412000264

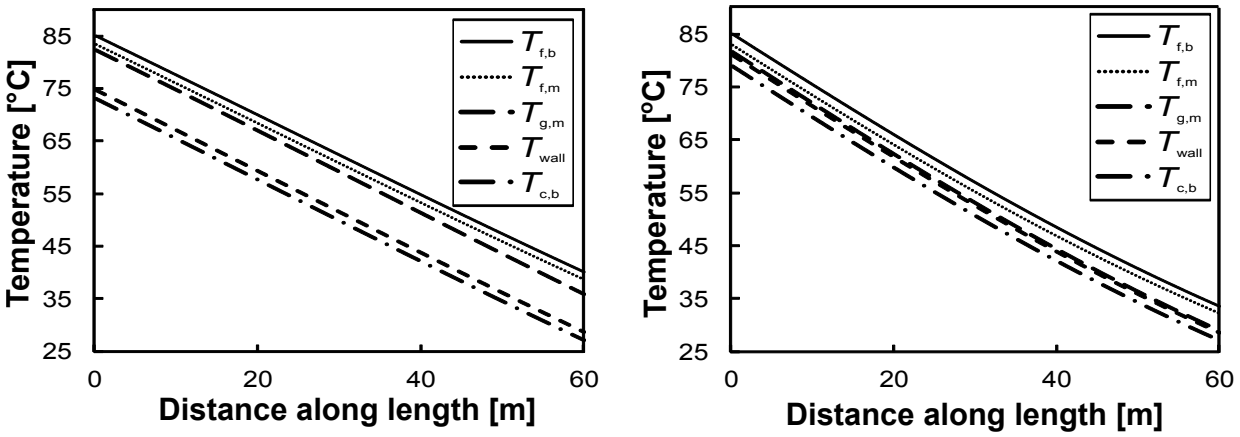

(a) PGMD

(b) CGMD

Figure 9: Temperature profiles in PGMD and CGMD systems. Simulation parameters set at baseline values (Table 1).

[6] S. Lin, N. Y. Yip, M. Elimelech, Direct contact membrane distillation with heat recovery: Thermodynamic insights from module scale modeling, Journal of Membrane Science 453 (2014) 498–515. doi:10.1016/j.memsci.2013.11.016.
URL http://www.sciencedirect.com/science/article/pii/S0376738813009010

[7] K. Lawson, D. Lloyd, Membrane distillation, Journal of Membrane Science 124 (1) (1997) 1–25. doi:10.1016/S0376-7388(96)00236-0.
URL http://linkinghub.elsevier.com/retrieve/pii/S0376738896002360

[8] D. Warsinger, J. Swaminathan, L. Maswadeh, J. H. Lienhard V, Superhydrophobic condenser surfaces for air gap membrane distillation, Journal of Membrane Science 492 (2015) 578–587. doi:10.1016/j.memsci.2015.05.067.
URL http://www.sciencedirect.com/science/article/pii/S0376738815005050

[9] J. Swaminathan, J. H. Lienhard V, Energy efficiency of sweeping gas membrane distillation desalination cycles, in: Proceedings of the 22nd National and 11th International ISHMT-ASME Heat and Mass Transfer Conference, IIT Kharagpur, India 2014, 2014.

[10] M. I. Hassan, A. T. Brimmo, J. Swaminathan, J. H. Lienhard V, H. A. Arafat, A new vacuum membrane distillation system using an aspirator: Concept modelling and optimization, Desalination and Water Treatment (accepted, 2015). doi:10.1080/19443994.2015.1060902.
URL http://www.tandfonline.com/doi/abs/10.1080/19443994.2015.1060902?journalCode=tdwt20#.VaCPydgtFZQ

[11] K. H. Mistry, R. K. McGovern, G. P. Thiel, E. K. Summers, S. M. Zubair, J. H. Lienhard V, Entropy Generation Analysis of Desalination Technologies, Entropy 13 (10) (2011) 1829–1864. doi:10.3390/

e13101829.
URL http://www.mdpi.com/1099-4300/13/10/1829/

[12] D. M. Warsinger, K. H. Mistry, H. W. Chung, K. G. Nayar, J. H. Lienhard V, Entropy generation of desalination powered by variable temperature waste heat, under review in Entropy, 2015.

[13] G. Zaragoza, A. Ruiz-Aguirre, E. Guillén-Burrieza, Efficiency in the use of solar thermal energy of small membrane desalination systems for decentralized water production, Applied Energy 130 (2014) 491–499.
URL http://www.sciencedirect.com/science/article/pii/S0306261914001603

[14] Global Water Intelligence, Global water intelligence and water desalination report 2014, http://desaldata.com/.

[15] J. Gilron, L. Song, K. K. Sirkar, Design for cascade of crossflow direct contact membrane distillation, Industrial & Engineering Chemistry Research 46 (8) (2007) 2324–2334. doi:10.1021/ie060999k.
URL http://pubs.acs.org/doi/abs/10.1021/ie060999k

[16] H. Lee, F. He, L. Song, J. Gilron, K. K. Sirkar, Desalination with a cascade of cross-flow hollow fiber membrane distillation devices integrated with a heat exchanger, AlChE Journal 57 (7) (2011) 1780–1795. doi:10.1002/aic.12409.
URL http://onlinelibrary.wiley.com/doi/10.1002/aic.12409/abstract

[17] H. Geng, H. Wu, P. Li, Q. He, Study on a new air-gap membrane distillation module for desalination, Desalination 334 (1) (2014) 29–38. doi:10.1016/j.desal.2013.11.037.
URL http://dx.doi.org/10.1016/j.desal.2013.11.037

[18] D. E. M. Warsinger, J. Swaminathan, J. H. Lienhard V, Effect of module inclination angle on air gap membrane distillation, in: Proceedings of the 15th International Heat Transfer Conference, IHTC-15, Paper No. IHTC15-9351, Kyoto, Japan August 2014.
URL http://web.mit.edu/lienhard/www/papers/conf/IHTC15-9351_Warsinger.pdf

[19] A. Cipollina, M. D. Sparti, A. Tamburini, G. Micale, Development of a membrane distillation module for solar energy seawater desalination, Chemical Engineering Research and Design 90 (12) (2012) 2101 – 2121. doi:http://dx.doi.org/10.1016/j.cherd.2012.05.021.
URL http://www.sciencedirect.com/science/article/pii/S0263876212002444

[20] D. Winter, J. Koschikowski, M. Wieghaus, Desalination using membrane distillation: Experimental studies on full scale spiral wound modules, Journal of Membrane Science 375 (1-2) (2011) 104–112. doi:10.1016/j.memsci.2011.03.030.
URL http://linkinghub.elsevier.com/retrieve/pii/S0376738811002067

[21] D. Singh, K. K. Sirkar, Desalination by air gap membrane distillation using a two hollow-fiber-set membrane module, Journal of Membrane Science 421422 (2012) 172 – 179. doi:http://dx.doi.org/10.1016/j.memsci.2012.07.007.
URL http://www.sciencedirect.com/science/article/pii/S0376738812005170

[22] L.-H. Cheng, P.-C. Wu, J. Chen, Numerical simulation and optimal design of agmd-based hollow fiber modules for desalination, Industrial & Engineering Chemistry Research 48 (10) (2009) 4948–4959. doi:10.1021/ie800832z.
URL http://pubs.acs.org/doi/abs/10.1021/ie800832z

[23] Z. Ma, T. D. Davis, J. R. Irish, G. D. Winch, Membrane distillation system and method, US Patent App. 12/694,757 (Jan. 27 2010).

[24] A. Alklaibi, N. Lior, Comparative study of direct-contact and air-gap membrane distillation processes, Industrial & engineering chemistry research (2007) 584–590.
URL http://pubs.acs.org/doi/abs/10.1021/ie051094u

[25] S. Agashichev, A. Sivakov, Modeling and calculation of temperature-concentration polarisation in the membrane distillation process (MD), Desalination 93 (1-3) (1993) 245–258. doi:10.1016/0011-9164(93)80107-X.
URL http://linkinghub.elsevier.com/retrieve/pii/001191649380107X

[26] Temperature and concentration polarization in membrane distillation of aqueous salt solutions, Journal of Membrane Science 156 (2) (1999) 265 – 273. doi:http://dx.doi.org/10.1016/S0376-7388(98)00349-4.
URL http://www.sciencedirect.com/science/article/pii/S0376738898003494

[27] H. Chang, J.-S. Liau, C.-D. Ho, W.-H. Wang, Simulation of membrane distillation modules for desalination by developing user's model on Aspen Plus platform, Desalination 249 (1) (2009) 380–387. doi:10.1016/j.desal.2008.11.026.
URL http://linkinghub.elsevier.com/retrieve/pii/S0011916409009229

[28] G. Zuo, R. Wang, R. Field, A. G. Fane, Energy efficiency evaluation and economic analyses of direct contact membrane distillation system using Aspen Plus, Desalination 283 (2011) 237–244. doi:10.1016/j.desal.2011.04.048.
URL http://linkinghub.elsevier.com/retrieve/pii/S0011916411003869

[29] S.A.Klein, Engineering equation solver version 9, http://www.fchart.com/ees/.

[30] J. Swaminathan, Numerical and experimental investigation of membrane distillation flux and energy efficiency, Master's thesis, Massachusetts Institute of Technology (2014).

[31] F. Al Marzooqi, M. Roil Bilad, J. Swaminathan, J. H. Lienhard V, H. Arafat, Flux measurements in novel membrane distillation configurations, in: Proceedings of The International Desalination Association World Congress on Desalination and Water Reuse, San Diego, CA, USA, 2015.

[32] G. P. Thiel, R. K. McGovern, S. M. Zubair, J. H. Lienhard V, Thermodynamic equipartition for increased second law efficiency, Applied Energy 118 (2014) 292 – 299. doi:http://dx.doi.org/10.1016/j.apenergy.2013.12.033.
URL http://www.sciencedirect.com/science/article/pii/S0306261913010325